Environmental Science Advances

ROYAL SOCIETY OF CHEMISTRY

PAPER

View Article Online
View Journal

Cite this: DOI: 10.1039/d5va00394f

Synthesis, weathering and machine learning modeling of nutrient-doped fast-weathering silicate minerals for carbon capture, utilization and sequestration (CCUS)

Asif Ali *[ab] and Rafael M. Santos [a]

Mineral carbonation is a promising carbon capture, storage and utilization (CCUS) technology that has enormous potential for capturing atmospheric CO_2 (a greenhouse gas) and converting it into environmentally stable products. Slow weathering of naturally occurring silicate minerals is a key challenge for mineral carbonation, as some minerals can take centuries to weather and convert leached calcium and magnesium cations into carbonates. A comprehensive literature review revealed that there is a scarcity of studies on fast weathering silicate minerals for mineral carbonation. Some silicates, such as akermanite and calcio-olivine minerals, have shown faster weathering capabilities. However, the doping of these minerals with plant nutrients to offer both organic and inorganic carbon capture benefits have not yet been investigated and signifies the novelty of the present research. The present research investigated the synthesis process of nutrient-doped akermanite and calcio-olivine *via* solid-state sintering methodology and the weathering capabilities of synthesized minerals compared with those of naturally occurring silicate minerals. A machine learning model is developed to help forecast the weathering capabilities of silicate minerals for deployment. X-ray diffraction (XRD), scanning electron microscopy (SEM), scanning electron microscopy-energy-dispersive X-ray spectroscopy (SEM-EDS), Brunauer–Emmett–Teller (BET), and inductively coupled plasma-mass spectrometry (ICP-MS) were used to characterize and analyze the performance of the synthesized minerals. The synthesis conditions of akermanite and calcio-olivine were adapted from the literature by tuning the temperature conditions for synthesizing these minerals, resulting in successful synthesis. SEM analysis helped elucidate the morphological characteristics of akermanite and calcio-olivine. During the sintering experiments, swelling of the calcio-olivine tablet was observed, which was confirmed by cracks in the fused calcio-olivine particles at one micrometer scale. The weathering experiments resulted in the release of calcium and magnesium cations, where fast-weathering silicate minerals resulted in faster release of alkaline earth metal cations, creating more opportunities for capturing atmospheric CO_2. The ICP-MS results also revealed the release of potassium cations, confirming that nutrients take part in the weathering process. The release of micro-nutrients is relatively fast, which opens a future research direction to investigate other methodologies of nutrient's incorporation during the synthesis process. The machine learning modeling results indicated fast weathering of synthesized silicate minerals compared with naturally occurring silicates, where calcio-olivine provided relatively more CO_2 sequestration than did akermanite. The results provide research insights and future research directions in the fast-weathering silicate mineral research area for the scientific community to fill potential knowledge gaps.

Received 1st November 2025
Accepted 20th January 2026

DOI: 10.1039/d5va00394f

rsc.li/esadvances

Environmental significance

Enhanced weathering of silicate minerals is widely studied, but research on nutrient-doped silicates for decarbonization and co agricultural use remains scarce. Understanding synthesis conditions, material properties, and leaching behaviour is important because controlled micro-nutrient release can support crops while reducing environmental losses. When plant roots are actively taking up nutrients, slow micro-nutrient release improves growth and minimizes losses through leaching. Key results show successful mineral synthesis confirmed through characterization, along with relatively rapid nutrient release. The work highlights opportunities to explore additional nutrient-incorporation methods during synthesis. Machine-learning modelling also suggests that nutrient-doped calcio-olivine relatively sequesters more CO_2 than naturally occurring akermanite.

[a]*School of Engineering, University of Guelph, Guelph, ON, N1G 2W1, Canada. E-mail: aali38@uoguelph.ca*

[b]*Department of Civil and Minerals Engineering, University of Toronto, Toronto, ON, M5S 1A4, Canada. E-mail: asifmunawar.ali@utoronto.ca*

Introduction

Anthropogenic activities in the past century have given rise to elevated levels of greenhouse gas emissions. Severe notable effects include ozone layer depletion, global warming, climate change, *etc.* These adverse changes in the environment are becoming the reason for the extinction of several living species. The unprecedented pace of technological and infrastructure development has caused the emission of greenhouse gases. Even if dangerous pollutant emissions are effectively reduced/eliminated, which is a difficult goal to achieve in the short-term, it would still not be sufficient to stagnate (and reverse) the negative effects caused by CO_2 emissions to the living ecosystem. In other words, the UN climate agreement goals[1] cannot be achieved only by reducing polluting emissions. This indicates that efforts are required farther than just limiting emissions.

There is an immediate urge for carbon capture, utilization, and sequestration (CCUS) from the atmosphere. Greenhouse gas emissions can be reduced by utilizing the potential of CCUS technologies.[2–4] The technologies designed for such systems are known as negative emission technologies (NETs).[5] Among these technologies, enhanced silicate weathering (ESW)[6] is considered to have significant potential for CO_2 capture. Naturally-occurring silicate minerals neutralize atmospheric CO_2, but their rate of weathering is very slow. This finding indicates that mineral carbonation should not only be emphasized for improving the weathering of natural silicate minerals[7] but also that attention should be given to industrial alkaline solid waste materials[8] and synthetic minerals with faster weathering rates.[9] The aim of ESW is to artificially increase the weathering rate of minerals to capture atmospheric CO_2 at an effective pace.[10] Some recent studies, which use alkaline silicate minerals to capture atmospheric CO_2 and accumulate inorganic carbon in soils, are mentioned below.

Renforth *et al.* who studied the role of urban soils as atmospheric CO_2 sinks, reported that the inorganic pathway of carbonation is approximately three times more effective than the organic pathway.[11] These findings indicate the significant role of fast-weathering silicate mineral synthesis in CCUS. As part of alkaline solid waste weathering, Washbourne *et al.* investigated CO_2 capture and sequestration in urban soils.[12] They reported that Mg- and Ca-based silicate minerals in demolished concrete weather at a faster rate.[12] This suggests that the synthesis of silicate minerals with swift weathering rates could focus on silicates rich in Ca and Mg. In another study, Manning *et al.* investigated carbonate precipitation in artificial soils by adding dolerite fines from basalt quarries blended with compost and finely grounded basalt to the soil.[13] They reported that the soil inorganic carbon (SIC) sequestration rate was 36.7 t CO_2 ha^{-1} at a depth of 1 meter.[13] This conclusion highlights the possible effective role of synthetic fast-weathering silicate minerals. The findings from these studies confirmed that the inorganic carbon sequestration pathway has significant potential for working as a tool in fighting global climate change. This inspired the synthesis of nutrient-doped fast-weathering silicate minerals to be produced in a net-negative manner, which, when mixed with agricultural soils, could not only capture and sequester atmospheric carbon but also utilize it by providing both environmental and agricultural benefits.

The storage of CO_2 includes geologic, oceanic, and mineral storage pathways. CO_2 geologic storage follows the same mechanism as that of storing fossil fuels in nature, where CO_2 is injected at a certain depth into a suitable underground geological stratum. It has a high storage capacity and is currently widely used for enhanced oil/gas recovery (EOR/EGR).[14,15] However, this geological CO_2 storage method has potential risks, including deformation of the geological structure, an increase in earthquakes, and acidification of groundwater.[16] Another hazard could be leakage through the CO_2 pipeline, which can cause suffocation to human beings near the storage site. Thus, geological sequestration can be considered for CCUS solutions as location-based technology, with the drawbacks of high incorporation costs and the need for post-storage monitoring.[17] Theoretically, the sequestration capacity of CO_2 in oceans is considerable, but the risks and concerns are even greater. Like geological sequestration, oceanic storage also requires the injection of CO_2 in deep oceans, with concerns of liquid CO_2 lake formation due to the supercritical and high-pressure state. The stored CO_2 may also volatilize back into the atmosphere; if not, it can acidify ocean water, which could destroy the marine ecosystem and devastate marine life.

Mineral carbonation, also known as CO_2 mineral storage or CO_2 mineralization, is a mechanism that imitates and accelerates the natural weathering process of rocks, in which CO_2 reacts with calcium- or magnesium-containing minerals and is permanently sequestered in the form of stable carbonates ($CaCO_3$/$MgCO_3$).[18,19] Minerals, which are susceptible to carbonation, can react with either CO_2 released from the effluent chambers of power plants or as a byproduct of industrial processes. Rapidly weathered minerals also contain an opportunity to capture and store atmospheric CO_2 naturally in the form of carbonates. The standard Gibbs free energy of CO_2 is much greater than that of carbonates, which indicates that carbonates are more stable forms of CO_2.[20] This method provides a safe and monitoring free solution for permanent CO_2 sequestration. Simultaneously, the products (carbonates) formed through mineral carbonation reduce the mining of limestone and could be used with other construction materials. Additionally, there are minimal uncertainties about the risk of CO_2 leakage with the mineral carbonation pathway of CCUS,[21] as carbonates are formed, which are thermodynamically stable and remain on the ground for geological time scales. Owing to these benefits, mineral carbonation has tremendous potential for industrial applications.

There are several natural minerals available as raw materials for CO_2 mineral storage, namely, wollastonite ($CaSiO_3$),[22–26] forsterite (Mg_2SiO_3),[27,28] tricalcium silicate,[29] and serpentine ($Mg_3Si_2O_5(OH)_4$).[30–34] Some other industrial solid waste materials can also be used for mineral carbonation, including waste gypsum,[35–37] fly ash,[38–40] steel slag,[41–43] blast furnace slag,[44–46] and demolished concrete.[47,48] Looking at the amount, availability,

and distribution of these natural minerals and industrial solid wastes, the quantity of these materials is abundant, widely available and distributed around the globe. According to a recent geological survey, the known reserves for wollastonite, forsterite, and serpentine are 300, 800, and 500 Mt, respectively, whereas the annual industrial solid waste outputs of gypsum, fly ash, steel slag, and blast furnace slag are 220, 1000, 240, and 390 Mt, respectively.[49] This fact reinforces the basic feasibility of the CCUS pathway of mineral carbonation. However, the energy-intensive and environmentally damaging nature of the mining process reduces the efficacy of natural minerals for carbonation. On the other hand, alkaline solid waste provides ready availability near industrial sites, intrinsic alkalinity, and increased reactivity for CO_2 mineralization.[50] Fig. 1 illustrates the concept process diagram of the present study, indicating the use of steel slag and cement clinkers to decarbonize hard-to-abate industries by fostering a circular economy. There are two distinct phases related to the weathering of minerals in soil: (i) the weathering of hard rocks in nature, which has broken them down and caused the formation of clays, loams, and sands, thereby forming soils; and (ii) the ongoing weathering of soil minerals, which release nutrients that are essential for crops. The weathering of minerals referred to in the first phase involves minerals that are found in various kinds of soils and parent materials of soils. The second phase focuses on the ions released from weathering minerals under specific conditions. As several portions of the world are intensified with agriculture, the amount of nutrients released through the weathering process becomes considerably smaller than those supplied by fertilizer applications. The weathering release of nutrients, both in tropical and temperate regions, is of vital importance in crop production and soil fertility.[51]

The kinetics and dynamics of the mineral carbonation process consist of an initial reaction stage where rapid dissolution of the mineral releases cations such as Mg^{2+} and Ca^{2+} in solution. During the intermediate stage of the mineral carbonation reaction, growth of the carbonate layer and nucleation occur. The rate of this stage is usually slow, as passivation of the surface layer follows. In the long term, mineral carbonation reaction kinetics are governed by the diffusion of cations through the product layer and the availability of CO_2 in the solution. Owing to product formation at the surface, the rate of reaction decreases. Keeping in view of the climate change solution and net-zero goals, the mineral

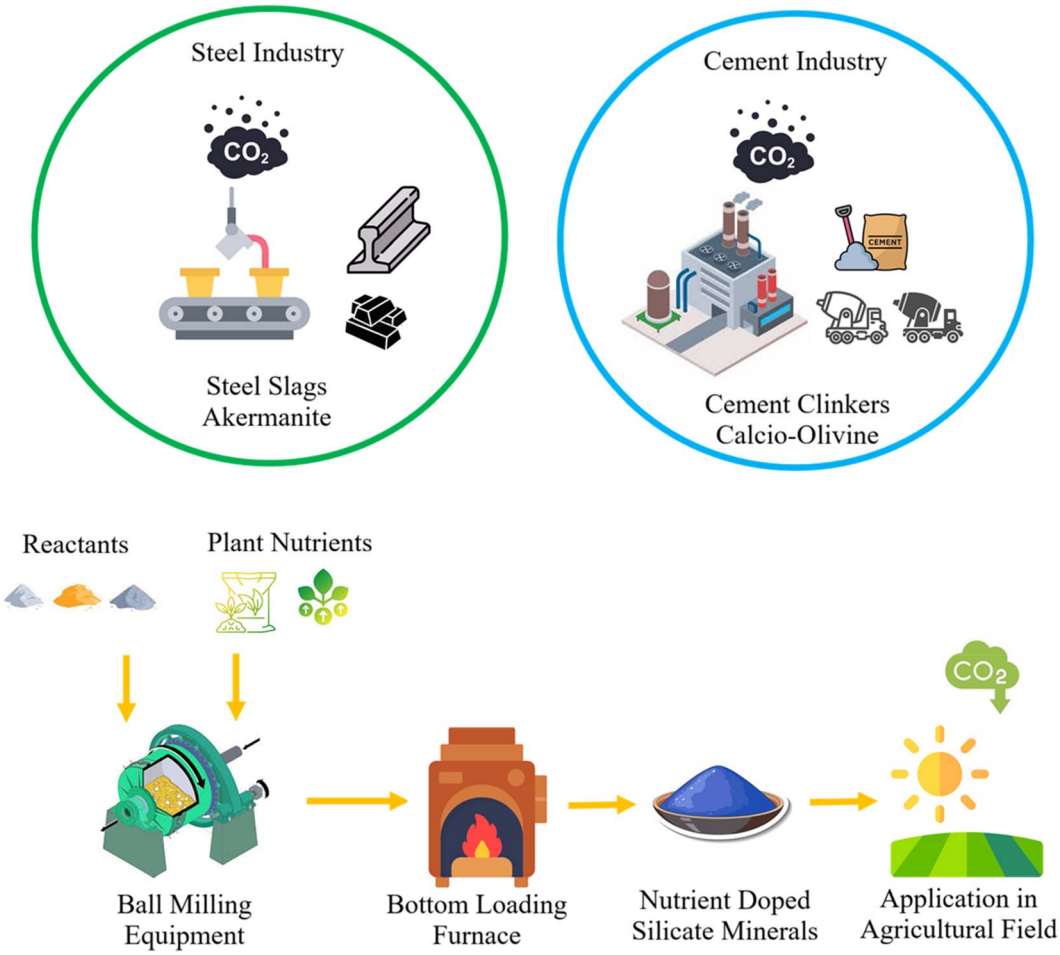

Fig. 1 The concept process diagram indicating syntheses of fast-weathering silicate minerals for atmospheric carbon capture, fostering a circular economy.

carbonation reactivity of minerals can be forecasted for a few decades to come, as predicting the reaction rate at geological time scales, such as centuries, will not be useful for combatting climate change. In summary, an effective mineral carbonation CCUS solution that can solve, for decades but not centuries, the increasing challenges of global warming is needed. The present work can aid the scientific community in closing the research gap concerning the synthesis conditions of fast-weathering minerals and the potential incorporation of micronutrients into these minerals for their prospective utilization in the mineral carbonation domain to mitigate the carbon footprint of hard-to-abate industries. The novelty of the present work lies in the study of the synthesis, weathering, and deployment of fast-weathering silicate minerals doped with plant nutrients as a solution to climate change. The development of a machine learning model for deployment modeling further innovates the investigation methodology, providing insights for atmospheric carbon sequestration in the coming decades.

Materials and methods

Naturally occurring silicate minerals exhibit slow weathering rates. The idea behind the present research project is to synthesize fast-weathering silicate minerals doped with plant nutrients not only to capture and sequester CO_2 but also to utilize it. A solid-state sintering methodology was used for the synthesis process. The technique and process parameters, including the sintering duration, temperature, milling time, and cooling method, were adapted from the literature[52] with minor adjustments. The synthesis conditions for the target minerals are presented in Table 1. The analytical grades of the constituent oxides (*i.e.*, MgO, CaO, and SiO_2) are used in stoichiometric quantities to synthesize the corresponding minerals. These oxides can be found abundantly in nature or produced *via* net-negative emission methods, keeping in view the objective of NETs. The target minerals are produced in batches of 5 g, with two batches of each mineral, to obtain sufficient material for characterization and carbonation tests. Milling operations are performed to ensure the mixing of ingredient oxides. The milled samples are pelletized by applying mechanical pressure to the powder mixture. Pellets are placed into the bottom loading furnace with the heat treatment and time conditions mentioned in Table 1.

Pellets are created before heat treatment to achieve the solid-state sintering process. The heat treatment temperatures are set below the melting points of the oxide ingredient, whereas pellet creation reduces the free surface area of the particles with increasing density. A platinum crucible was used to hold the pellet inside the bottom loading furnace. The synthesis process was repeated three times, synthesizing three replicates of akermanite and calcio-olivine each, to analyze the consistency of the synthesis process.

Table 1 Synthesis conditions for fast-weathering silicate minerals

Mineral	Temperature (°C)/time (hours)	Milling time (hours)	Cooling method
Akermanite	1200/48	2	Natural convection
Calcio-olivine	1300/24	2	Natural convection

XRD analysis (using XRD equipment (Malvern Panalytical, (Almelo, The Netherlands) Empyrean XRD Diffractometer)) was conducted on a heat-treated mixture to gauge the success of the synthesis process and characterization of the samples.[53] If the target mineral is above 70% of the total composition, the synthesis process is considered adequate, and further analysis and characterization are performed on the samples.

Plant nutrients are doped in the process of synthesizing minerals where nutrient powders, K_2MoO_4 (potassium molybdate) and P_4O_{10} (phosphorus pentoxide), are added at 0.1% (of the target mineral weight) with the constituent oxides before being milled so that all the reactant mixtures are properly blended and pelletized and then heated to prepare the required target minerals with plant nutrients. Scanning electron microscopy (SEM) analysis was conducted on both akermanite and calcio-olivine samples *via* an FEI (Hillsboro, OR, USA) Inspect S50 instrument to gain in-depth insights into the morphologies of synthesized minerals.[54] The phase diagram for the target synthesized minerals is shown in Fig. 2. The ternary diagrams here represent akermanite ($Ca_2MgSi2O_7$) with 41% CaO, 15% MgO, and 44% SiO_2 by weight and calcio-Olivine (Ca_2SiO_4) with 65% CaO and 35% SiO_2 by weight.

The synthesized mineral samples of akermanite and calcio-olivine were characterized *via* Brunauer–Emmett–Teller (BET) surface area analysis *via* N_2 adsorption at 77 K *via* a physisorption analyzer (Autosorb iQ). Before the adsorption measurements were taken, both minerals were degassed under vacuum at 120 °C with a 30 minute soaking time and at 350 °C with a 300 minute soaking time. Fig. 3 shows the adsorption isotherms of synthesized minerals. Three samples of each akermanite and calcio-olivine were tested for surface area *via* the multipoint Brunauer–Emmett–Teller method. The average surface area of the synthesized akermanite is 15.69 $m^2\ g^{-1}$, and that of the synthesized calcio-olivine is 11.01 $m^2\ g^{-1}$.

Weathering experiments were conducted to analyze the leaching capacity of synthesized minerals. In addition to akermanite and calcio-olivine, other minerals that have already gained attention in the mineral carbonation industry, including wollastonite, feldspar, olivine, and serpentine, were included in the weathering study. Two replicates of akermanite and calcio-olivine (each) were prepared for weathering experiments. Two grams of each mineral was added to 13.3 ml of oxalic acid. The pH of oxalic acid was measured as 2.33. These samples were placed in a reciprocating shaker at a reciprocating speed of 250 strokes per minute for 24 hours. Centrifugation was conducted at 3470 rpm for 10 minutes, and at the end of the experiment, the particles were allowed to settle. The leachate was collected, and the weathering sample tube was filled with oxalic acid again to conduct the weathering experiment. The leachates were conducted six times in total, first three after 24 hours and last three after 48 hours each. The interval between placing the samples in a reciprocating shaker and centrifuging the leachate out is considered the "weathering stage" in this study.

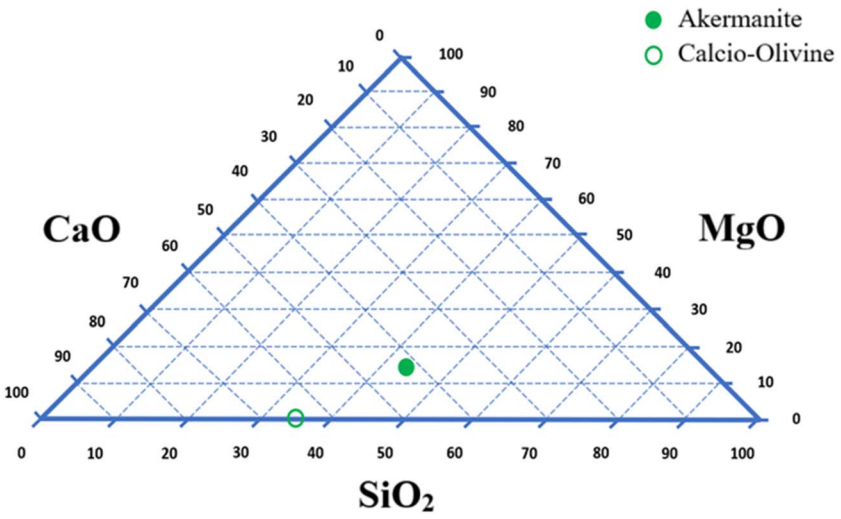

Fig. 2 Phase diagram of the target fast-weathering synthetic minerals, akermanite and calcio-olivine.

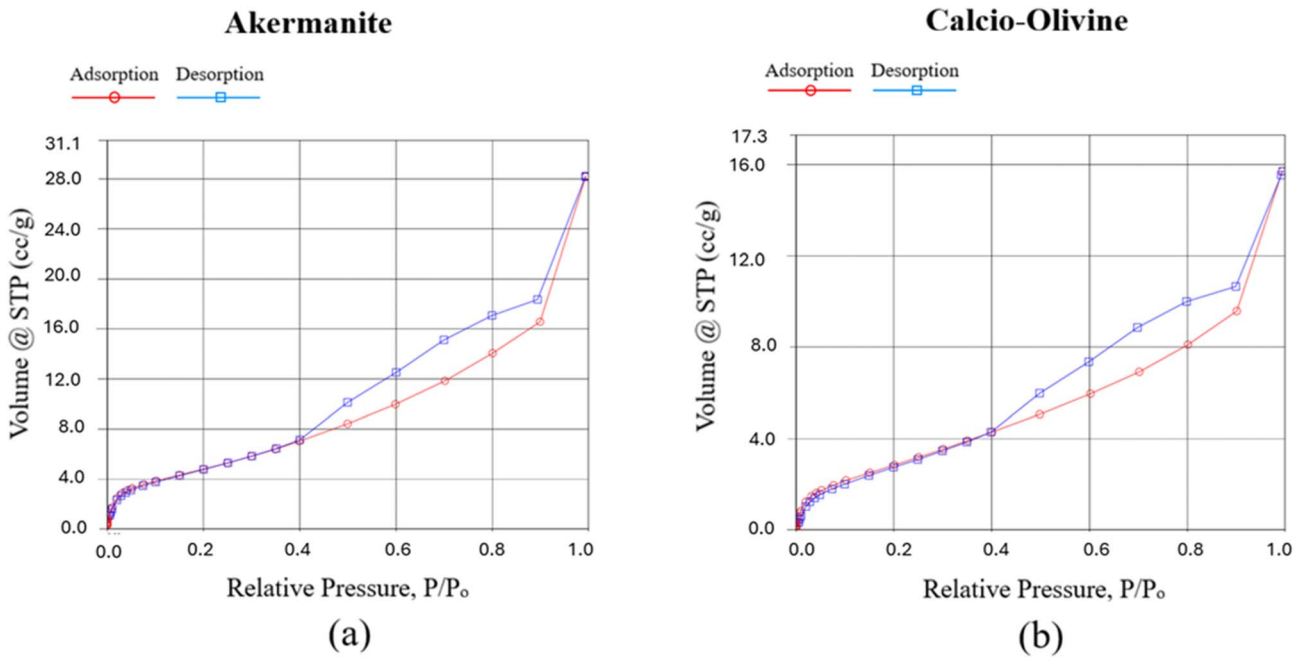

Fig. 3 Adsorption isotherms of synthesized minerals (a) akermanite and (b) calcio-olivine, characterized by N_2 adsorption at 77 K.

Therefore, there are 6 stages, the first three consisting of 24 hours and the remaining three consisting of 48 hours each. At the end of the six reciprocating runs, the last leachate was collected *via* slow filter paper and syringe filter, where the solids were dried and retrieved by placing the filtered samples in the oven for 24 hours at 60 °C.

The soluble element concentration in aqueous solution (comprising subsequent minerals and oxalic acid) was analyzed and quantified *via* ICP-MS (Inductively Coupled Plasma-Mass Spectrometry) (NexION, PerkinElmer, Waltham, MA, USA). Two hundred milliliters of each filtered sample was diluted with Milli-Q water containing 2 ml of nitric acid and 10 ppm Be or In as the internal standard.

A machine learning model was developed on the basis of the composition and weathering data available in the literature (Haque *et al.*, 2023). The model was trained on data from 12 minerals, including albite, anorthite, bytownite, oligoclase, k-feldspar, andradite, fayalite, forsterite, augite, enstatite, wollastonite, and lizardite, to forecast the weathering of synthetic akermanite and calcio-olivine. Eqn (1) was used to evaluate $\log A$, which was then used in eqn (2) to calculate $\log W_r$.

$$\log A = \log K + \frac{E \times 1000}{2.3025 \times 8.314 \times 298.15} \quad (1)$$

$$\log W_r = \log A - \frac{E \times 1000}{2.3025 \times 8.314 \times T} - n_{H^+} \times \mathrm{pH} \quad (2)$$

These factors were calculated *via* widely cited weathering rates of several minerals, as indicated in the investigation conducted by Palandri and Kharaka (2004). This regression model machine learning algorithm uses a random forest model and is novel because it utilizes the composition and weathering data of minerals to predict the weathering rates of synthetic minerals. The trained model predicts $\log K$, E, and n_{H^+} values at a particular pH for the input mineral composition, which is used to predict $\log A$, which is then used to predict the $\log W_r$. This model is used to predict the weathering rates of synthesized akermanite and calcio-olivine over a pH range of 3–9. Table 2 lists the mineral compositions of the minerals on the basis of the number of atoms present in a molecule, where $\log K$, E, and n_{H^+} data are retrieved from Haque *et al.* (2023). The developed machine learning model predicts $\log K$, E, and n_{H^+} values for synthesized minerals, akermanite and calcio-olivine, as shown by the Mathematica code in SI 7A. These values are used in eqn (1) and (2) to produce $\log A$ and $\log W_r$ values for akermanite and calcio-olivine.

Another mathematical model was developed for predicting prospective CO_2 sequestration by the application of 1 tonne per hectare per year of synthetic silicate minerals (akermanite and calcio-olivine) and naturally occurring silicate minerals (oligoclase, k feldspar, and enstatite) for 76 years starting from 2025–2100, assuming a constant diameter of particles of 100 μm. It is important to evaluate the time required (t) in years to weather/dissolute any given mass of silicate mineral reaching 100%, for which a shrinking core model can be used, as shown in eqn (3).

$$X(t) = \frac{{D_0}^3 - (D_0 - 2W_r V_m t)^3}{{D_0}^3} \quad (3)$$

$$t = \frac{D_0}{2W_r V_m} \text{ at } 100\% \text{ dissolution} \quad (4)$$

where D_0 represents the initial diameter of the mineral particle in meters, W_r indicates the weathering rate in mol m^{-2} s^{-1}, and V_m denotes the molar volume in m^3 mol^{-1}. Eqn (4) defines the time (in years) required to dissolve a particle to 100%, for which the value of $X(t)$ reaches 1.

The assumptions of the shrinking core model for the mineral carbonation process include that the reaction proceeds with the shrinking of the unreacted mineral core and the formation of carbonate products with a surrounding layer. The reaction zones can be divided into three categories: unreacted cores, reaction zones, and product layers. The reaction control mechanisms may include surface reaction kinetics, diffusion of cations and CO_2 through thin fluid films, and diffusion through the product layer. For the present mathematical modeling, the particle size is assumed to be uniform, and all the particles have a spherical shape for simplicity. The rationale of using shrinking models for forecasting carbonate formation includes their practical application to scaling, ease of mathematical representation, well-defined reaction zones and control mechanisms. This model is also in very close proximity to the experimental behavior of the mineral carbonation process.

Results and discussions

The synthesis process of akermanite and calcio-olivine was conducted to produce fast-weathering nutrient-doped minerals for carbon mineralization and to act as a fertilizer agent for agricultural crops. Following the heat treatment process, XRD analysis of synthesized akermanite was conducted, and the results were successful, as shown in Fig. 4, while the XRD diffractograms of calcio-olivine are shown in Fig. 5. Both figures describe the phase identification process. The target minerals were synthesized on the basis of the XRD results, which revealed that more than 70% of the sintered powder was akermanite or calcio-olivine. The remainder of the sintered powder included

Table 2 Mineral composition, $\log K$, E, and n_{H^+} data (Haque *et al.*, 2023)

Mineral	Chemical formula	Composition								$\log K$ (mol m^{-2} s^{-1})	E (kJ mol^{-1})	n_{H^+}
		Ca	Mg	Si	Na	Al	K	Fe	Ti			
Albite	$NaAlSi_3O_8$			3	1	1				−10.2	65	0.46
Anorthite	$CaAl_2Si_2O_8$	1		2		2				−3.5	16.6	1.41
Bytownite	$(Ca,Na)[Al(Al,Si)Si_2O_8]$	0.5		2.5	0.5	1.5				−5.85	29.3	1.02
Oligoclase	$(Ca,Na)(Al,Si)_4O_8$	0.5		2	0.5	2				−9.67	65	0.46
K-feldspar	$KAlSi_3O_8$			3		1	1			−10.1	51.7	0.5
Andradite	$Ca_3Fe_2Si_3O_{12}$	3		3				2		−5.2	94.4	1
Fayalite	Fe_2SiO_4			1				2		−4.8	94.4	1
Forsterite	Mg_2SiO_4		2	1						−6.85	67.2	0.47
Augite	$(Ca,Na)(Mg,Fe,Al,Ti)(Al,Si)_2O_6$	0.5	0.25	1	0.5	1.25		0.25	0.25	−6.82	78	0.7
Enstatite	$Mg_2Si_2O_6$		2	2						−9.02	80	0.6
Wollastonite	$CaSiO_3$	1		1						−5.37	54.7	0.4
Lizardite	$Mg_3S_{i2}O_5$		3	2						−5.7	75.5	0.8
Akermanite	$Ca_2MgSi_2O_7$	2	1	2								
Calcio-olivine	Ca_2SiO_4	2		1								

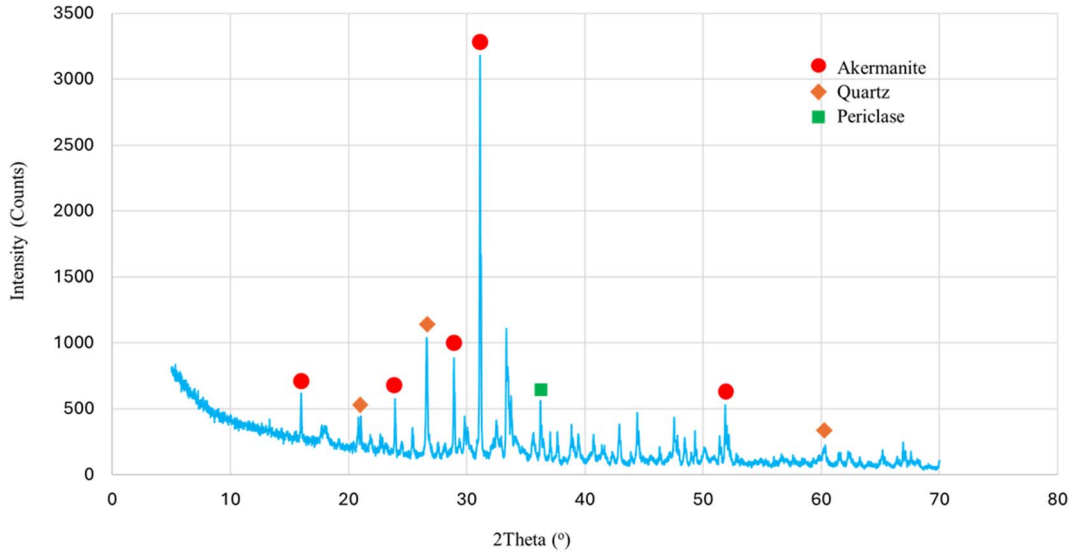

Fig. 4 XRD diffractograms of synthesized akermanite detecting akermanite (major phase), quartz (minor phase), and periclase (minor phase).

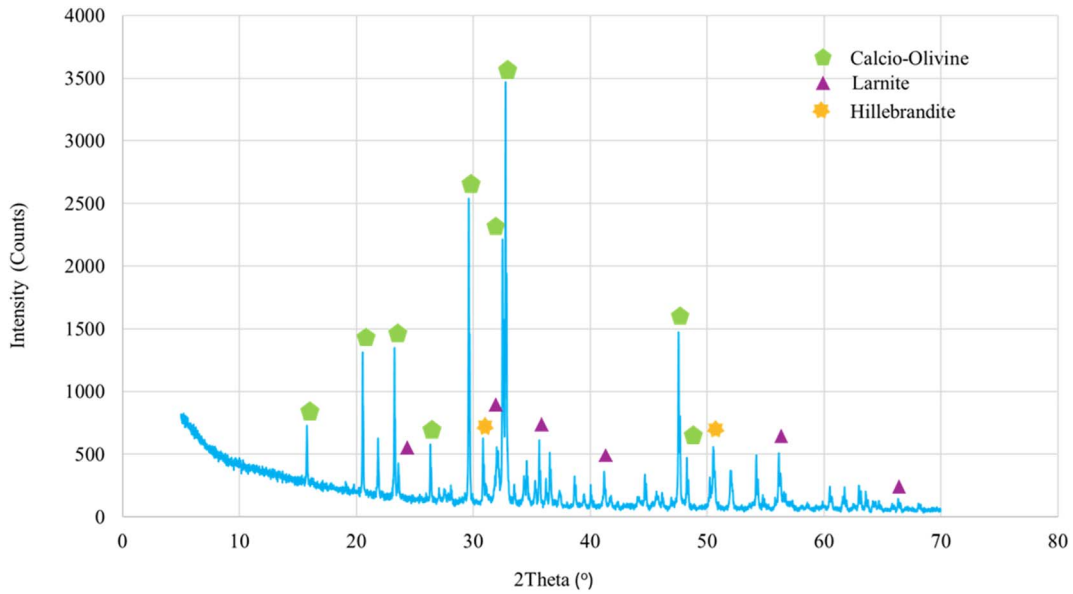

Fig. 5 XRD diffractograms of synthesized calcio-olivine detecting calcio-olivine (major phase), larnite (minor phase), and hillebrandite (minor phase).

phosphorous pentoxide, calcium molybdate, dipotassium tricalcium trisilicate, and a few unreacted ingredients, such as periclase (MgO), quick lime (CaO), and quartz (SiO_2). As the synthesis conditions reported in the literature require some adaptations, a future research pathway for finding the optimum synthesis conditions for fast-weathering silicate minerals is needed. Tables 3 and 4 present the XRD results for akermanite and calcio-olivine phase identification, respectively.

Given the importance of scientific consistency, the sintering experiments were repeated three times, and XRD was conducted, resulting in consistent and successful target mineral synthesis. Five milligrams of phosphorus pentoxide (P_2O_5) and potassium molybdate (K_2MoO_4) were doped into the ingredient mixture powder (5 g) of akermanite and calcio-olivine as nutrients for the plants. Separate samples were prepared with 10 times the amount of doped nutrients (50 mg) to identify their presence in the synthesized minerals. The XRD results revealed the presence of unreacted phosphorous pentoxide, while potassium from $KMoO_4$ was likely disintegrated and formed dipotassium tricalcium trisilicate, whereas molybdenum might have reacted with calcium ions to form calcium molybdate. Molybdenum is rarely found in any of the known silicate minerals. The compatibility of molybdenum in silicate crystal structures is less likely owing to its ionic radius, charge

Table 3 Akermanite XRD phase identification

Phase	h	k	l	Angle (° 2θ)	d (nm)	Intensity (deg*cts)	Relative intensity (%)
Akermanite	2	1	1	31.240	0.2873	403.3661	100
Quartz (SiO_2)	1	−1	1	26.5949	0.3351	117.0118	29.01
Periclase (MgO)	2	0	0	42.8996	0.2108	27.0755	6.71
Calcite	1	−1	−4	29.3529	0.3042	39.5661	9.81
Magnesite	1	−1	−4	32.5111	0.2753	36.5639	9.06

Table 4 Calcio-olivine XRD phase identification

Phase	h	k	l	Angle (° 2θ)	d (nm)	Intensity (deg*cts)	Relative intensity (%)
C_2S (Gamma)	1	2	1	32.8023	0.2730	335.8670	100
C_2S (Beta)	1	0	−3	32.0446	0.2792	75.1140	22.36

intensity, geochemical behavior, or synthesis conditions, such as temperature and pressure.

During the sintering experiments, heat treatment caused the calcio-olivine sample tablet to swell, whereas this behavior was absent in the akermanite case. Research has revealed that during the sintering process of calcio-olivine, hillebrandite (Dai, 1995) is formed, leading to swelling of the sintered tablet. This behavior can help in understanding the density, microstructure and properties of synthesized minerals.

Scanning electron microscopy was used to analyze the morphology of the synthesized minerals. Fig. 6 shows SEM images of three synthesized replicate samples of akermanite, which were snapped at resolutions of 1000× (top), 100 00× (middle), and 500 00× (bottom). SEM image analysis of the samples also validated the consistency of the synthesis process, which was evident from the regularity of the mineral texture for all three samples at a given resolution. At 1000× resolution, all three akermanite samples indicate the presence of a few chunks of particles agglomerated together. By zooming to 100 00×, all three samples start indicating the signs of the solid-state sintering process, as individual particles fuse with each other. As the samples are further zoomed to 500 00×, visible signs of coalescence are found with blunt and indistinct particles.

SEM images of three synthesized replicate samples of calcio-olivine snapped at resolutions of 1000× (top), 100 00× (middle), and 500 00× (bottom) (Fig. 7). For any specific resolution, the morphology of the calcio-olivine samples also shows consistency, validating the success of the synthesis experiments. At

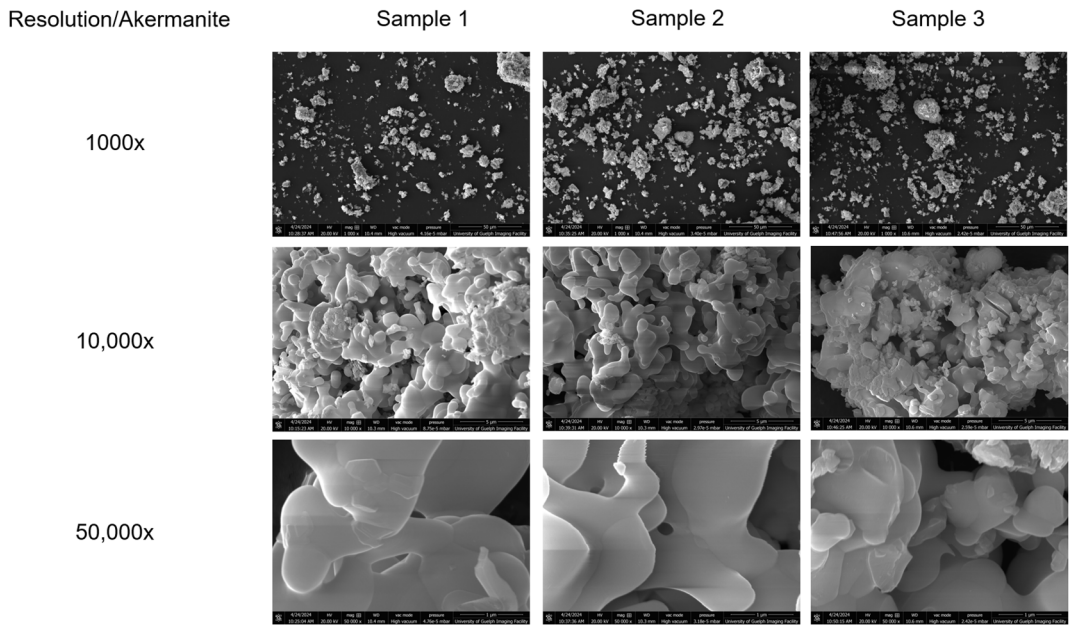

Fig. 6 Akermanite SEM images of three replicate synthesized samples; the top row shows images at 1000× resolution, the middle row represents a resolution of 10 000×, and the bottom row represents a resolution of 50 000×.

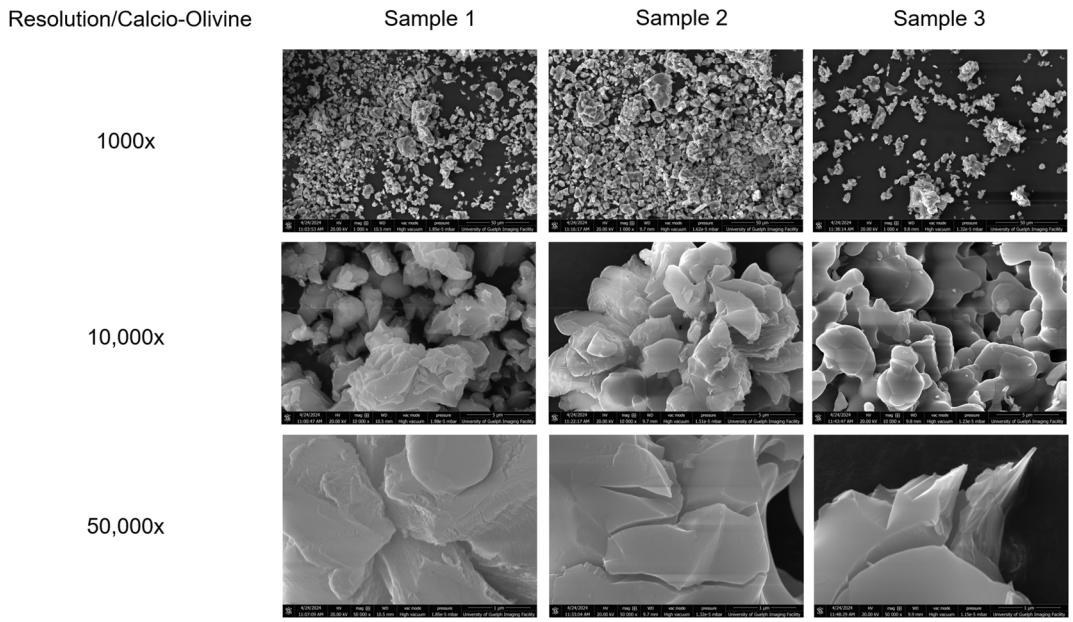

Fig. 7 Calcio-Olivine SEM images of three replicate synthesized samples; the top row indicates images of 1000× resolution, the middle row represents a resolution of 10 000×, and the bottom row represents 50 000× resolution.

1000× resolution, chunks of sharp-edged particles joined together can be observed. At 100 00× resolution, the signs of the particle sintering process become imminent, as these strident-edged particles are connected with each other, where the common boundary between the particles is losing shape, and the particles fuse together. The resolution of 500 00× shows a closer look into the fused agglomeration of particles. In contrast to the akermanite particles, the sharper edges of the calcio-olivine particles are evident in all three samples at this resolution. An interesting observation at 500 00× resolution is the presence of cracks in the calcio-olivine particles. This finding can be attributed to the swelling of the calcio-olivine observed while the heat treatment synthesis process was conducted. These cracks could validate the swelling observed during the experiments. The formation of hillebrandite (the hydrate of calcio-olivine) indicates the possible soaking of moisture from the environment, causing the particles to crack upon heating, as moisture evaporates. The presence of MgO in the ingredients of akermanite might have reduced the moisture soaking tendency of the other ingredients, which is why neither swelling of the akermanite tablet nor any cracks can be observed in the 500 00× resolution of the akermanite particles (Fig. 6). However, the presence of cracks and swelling of calcio-olivine tablets upon heat treatment require further research.

Fig. 8 and 9 represent the mineral characterization of synthesized akermanite and calcio-olivine samples, respectively, through SEM-EDS imaging. For both sample types, the analytical process of imaging consisted of the sample image at a 100 μm resolution (top), followed by a 10 μm resolution of a porous focus (upper middle), a 10 μm resolution of dark focus (lower middle), and a 10 μm resolution of lighter focus on the captured image (bottom). As shown in Fig. 8, the second portion (upper middle) focuses on a porous region and analyzes the elemental composition of six data points. There were a few darker spots identified in this focus, as represented by data points 001 and 005. The elemental compositions at these two points are quite similar, indicating that magnesium is present in relatively large quantities, followed by calcium, silica, potassium, phosphorus, and molybdenum. Data points 002, 003, 004, and 006 are focused on the lighter patches of akermanite sample powder, where the elemental composition graph is quite similar. These points have more silica and calcium present, followed by smaller quantities of magnesium, molybdenum, and potassium.

The third part of Fig. 8 (lower middle) analyzes one of the darker regions of the akermanite SEM image. Six data points and one rectangular cross-section are considered to analyze the elemental composition of akermanite. Data points 001 and 004 are pinpointed at darker shades, and the elemental composition graph indicates the presence of more magnesium than other elements. Data points 002 and 005 indicate lighter shades, where the elemental composition shows the presence of prevalent calcium and silica. Data points 003 and 006 and cross section 007 are grayish shades, somewhere in between the dark and lighter spots, and the elemental composition here reveals the dominance of silica oxide over other constituent elements. The fourth portion of Fig. 8 (bottom) shows one of the lighter regions of the akermanite SEM image. Four data points and one cross-sectional area were considered to analyze the elemental composition of the lighter focus of akermanite. Data point 003 focused on the darker spot where magnesium was prevalent, whereas all other data points and areas analyzed brighter spots where magnesium was present but where calcium and silica were dominant alongside. The darker spots on the focused light agglomeration of the synthesized mineral could indicate the presence of magnesium during akermanite formation. This

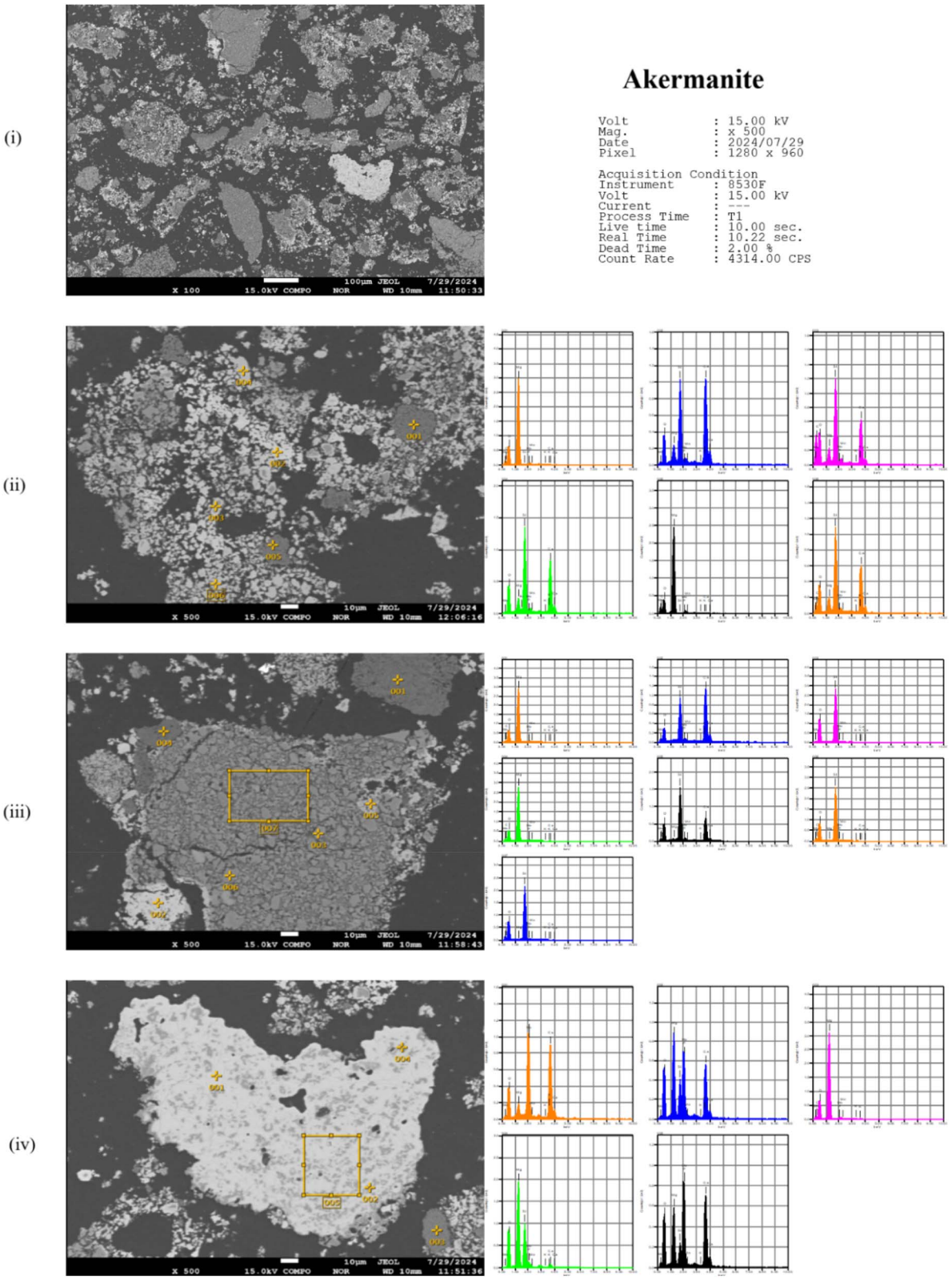

Fig. 8 SEM-EDS images of akermanite samples at 100 μm resolution (top), 10 μm resolution of the porous focus (upper middle), 10 μm resolution of the dark focus (lower middle), and 10 μm resolution of the light focus (bottom).

SEM-EDS analysis makes sense, as magnesium is therefore lighter in weight, represented by the darker portions of the SEM image. Calcium and silica are relatively heavier and represent brighter portions of the akermanite SEM image. Some portions that are very dark might represent unreacted magnesium, whereas very bright portions could represent unreacted silica

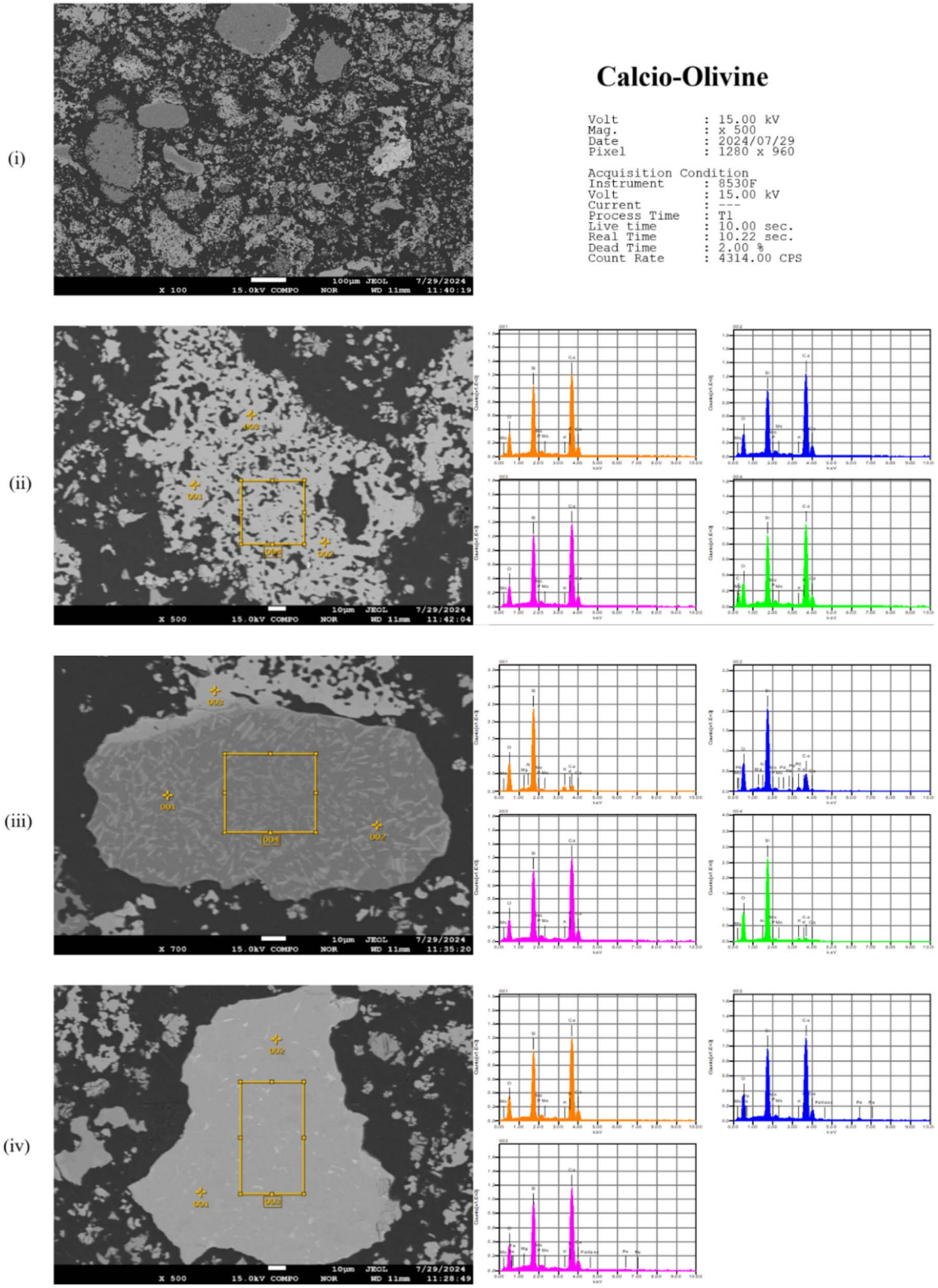

Fig. 9 Calcio-olivine SEM-EDS image samples at 100 μm resolution (top), 10 μm resolution of porous focus (upper middle), 10 μm resolution of dark focus (lower middle), and 10 μm resolution of light focus (bottom).

and calcium. Since the quantities of potassium and molybdenum were very small, these elements were not clearly identified *via* SEM-EDS; however, their presence was indicated.

As shown in Fig. 9, the second part (upper middle) corresponds to a porous section of the SEM image, where the elemental composition is identified by three data points and a rectangular cross-section. This porous section of the image is brighter in color and indicates the presence of calcium and silica, followed by potassium, molybdenum, and phosphorous. The third part (lower middle) shows a darker portion, which is characterized by three data points and a rectangular cross-section. All the darker portions of the section (lower middle) in Fig. 9 show the dominance of silica, followed by calcium and other micronutrients. For comparison, data point 003 was used to analyze the lighter portion of the section (lower middle), which suggested the prevalence of calcium over silica and micronutrients. The fourth part (bottom) highlights the lighter sections of the SEM image shown in Fig. 9, where the elemental composition is characterized by two data points and one rectangular cross-section. Calcium, which is heavier in atomic weight, dominates the lighter sections of the SEM image. Some even brighter spots might indicate the presence of molybdenum, which is also heavier than calcium.

Weathering experiments have been conducted on nutrient-doped akermanite and calcio-olivine samples to gauge how fast the weathering of calcium and other nutrients occurs for the synthesized minerals. For comparison with the existing mineral carbonation-trending minerals on the market, olivine, serpentine, wollastonite, and feldspar samples were included in the weathering study. The leaching experiments yielded the leached calcium concentration (mg l^{-1}) from two sample replicates of akermanite ($Ca_2MgSi_2O_7$), two sample replicates of calcio-olivine (Ca_2SiO_4), wollastonite ($CaSiO_3$), and feldspar ($CaAl_2Si_2O_8$) through six weathering stages, as shown in Fig. 10. As expected, the weathering of minerals decreases as time passes, as the active sites of the minerals are already leached before, and it becomes difficult to weather more stable atoms.

Both replicates of akermanite and calcio-olivine yielded the highest concentrations of calcium, which is the key agent in atmospheric carbon sequestration. By examining the chemical composition of the studied minerals, one can simply argue that one molecule of both akermanite and calcio-olivine consists of two atoms of Ca, whereas wollastonite and feldspar both have only one Ca atom. The ICP-MS concentration of Ca shown in Fig. 10 indicates far more than double the weathering of Ca in the case of akermanite and calcio-olivine compared with wollastonite and feldspar.

Fig. 10 suggests that in weathering stage 1, the concentration of Ca leached from akermanite samples was 3.5 times greater than that of their feldspar mineral counterparts. Compared with wollastonite mineral, calcio-olivine leached 5.48 times more Ca in stage 1. For weathering stage 2, akermanite weathered 28.6 times more Ca than feldspar did, whereas calcio-olivine weathered 18.14 times more Ca than wollastonite did. In weathering stage 3, akermanite leached 15.5 times more Ca than feldspar did, whereas calcio-olivine leached approximately 7 times more Ca than wollastonite did. For weathering stages 4, 5, and 6, the weathering of Ca is similar for all the studied minerals. The possible reason is that the Ca ions leached in stages 1, 2, and 3 were prone to weathering, and the leaching rate decreased in later stages owing to the increased number of stable atoms or the unavailability of Ca atoms for weathering. Fig. 10 explains how fast the weathering of synthesized akermanite and calcio-olivine is compared to the existing minerals. Both akermanite and calcio-olivine weathered many more Ca atoms than feldspar and wollastonite did, respectively, with the

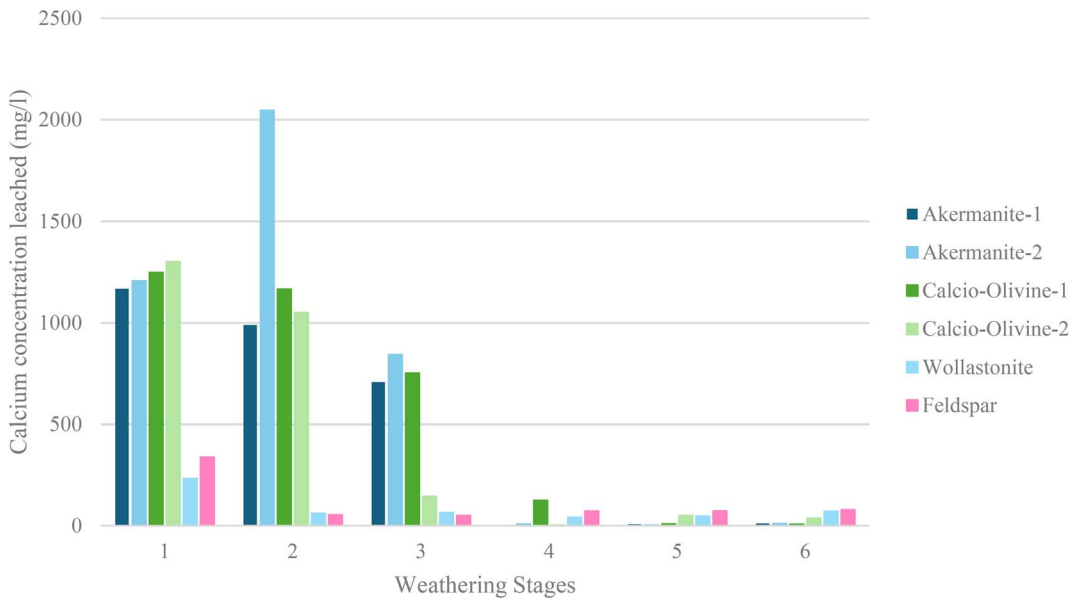

Fig. 10 Leached calcium concentration (mg l^{-1}) from two sample replicates of akermanite and two sample replicates of calcio-olivine, wollastonite, and feldspar through six weathering stages.

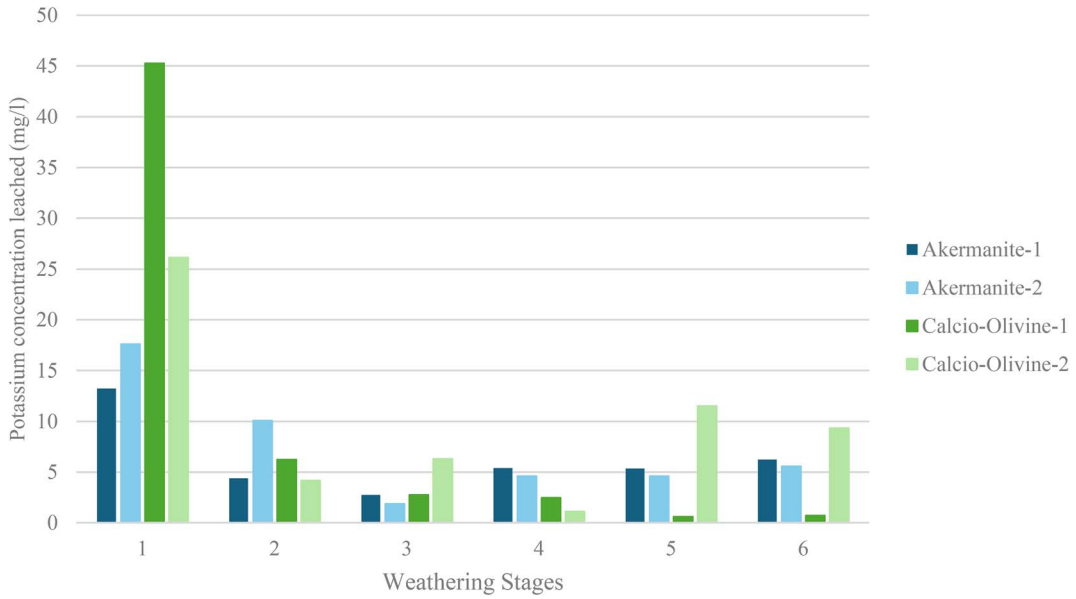

Fig. 11 Leached potassium concentration (mg l^{-1}) from two sample replicates of akermanite and two sample replicates of calcio-olivine through six weathering stages.

same weathering time. Producing fast-weathering silicate minerals through green energy sources can significantly help reduce the carbon footprint, especially for hard-to-abate industries such as steel, cement, and mining.

Fig. 11 shows the potassium concentration leached from weathering samples of akermanite and calcio-olivine. The nutrient doping of synthesized minerals included potassium molybdate (K_2MoO_4). An important research question is whether these doped nutrients leach during weathering, as this topic is important for the prospective use of these synthetic silicates in the net-negative fertilizer industry. The ICP-MS results indicate the release of potassium cations into the solution upon weathering, where calcio-olivine released more potassium than did akermanite in the first stage, whereas in the other stages, both minerals released almost the same amount of potassium. The variation in the amount of leached potassium from calcio-olivine, compared with akermanite, can be attributed to the chemical composition of silicate minerals. MgO is present as an ingredient in akermanite, which could restrain few cations of potassium from leaching. The dissolution–

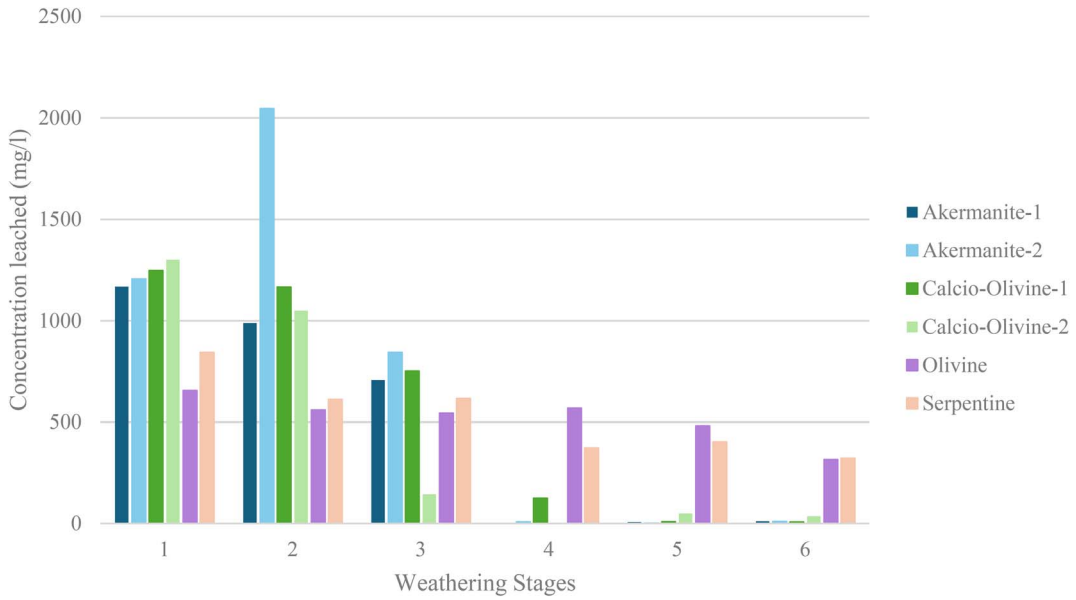

Fig. 12 ICP-MS results indicating the leaching of calcium from replicate samples of akermanite and calcio-olivine each and the leaching of magnesium from olivine and serpentine.

reprecipitation dynamics of akermanite may hinder potassium leaching, as MgO is present there. This is not the case with calcio-olivine, as it does not contain any MgO. This understanding is also supported by the published literature (Ma *et al.*, 2023, Jalali *et al.*, 2022). The leaching of potassium is a positive indicator of the weathering process of synthesized minerals. This opens up further research directions for investigating the doping of other plant nutrients into silicate minerals and studying their leaching behavior.

Another interesting leaching analysis approach is to compare the weathering outcomes of olivine (Mg_2SiO_4) and serpentine ($Mg_3Si_2O_5(OH)_4$), which are magnesium-silicate minerals. Fig. 12 shows the leached concentrations of magnesium from olivine and serpentine, which are compared with the leaching of calcium from calcio-olivine and akermanite, respectively. Magnesium silicate minerals have 2 atoms of Mg in a single molecule of olivine and 3 atoms of Mg in one molecule of serpentine, whereas synthesized calcium-based silicate minerals have 2 atoms of Ca in a single molecule each of akermanite and calcio-olivine. It looks like a fair comparison, on the basis of the presence of calcium and magnesium present in the ingredients of synthesized calcium silicate minerals and naturally occurring magnesium silicate minerals. The leaching results indicate higher concentrations of calcium leaching from synthetic calcium-based silicate minerals than from their naturally occurring magnesium-based silicate minerals in the first three stages of the weathering experiments. In the last three stages, synthetic minerals leach marginal amounts of calcium, resulting in the fast weathering of calcium-based silicate minerals. The concentration of leached magnesium or calcium indicates the prospective CO_2 capture capability of the minerals, as these Mg and Ca cations react with atmospheric CO_2 to form their respective carbonates. As compared to calcio-olivine, akermanite leached calcium faster which is evident by the larger specific surface area of akermanite particles than calcio-olivine, also indicated by BET and SEM analyses.

While comparing the leaching behavior of magnesium silicate minerals in the first three stages, serpentine leaches more magnesium cations than olivine does, which makes sense, as serpentine contains more magnesium atoms than olivine does in its molecule. However, for the last three stages, olivine dominated magnesium leaching over serpentine leaching. The presence of hydride in the serpentine molecule, which is not present in the olivine molecule, potentially causes this decrease in magnesium leaching in the later stages of weathering. Future research could identify and synthesize fast-weathering magnesium-based silicate minerals and investigate their leaching behavior.

Fig. 13 compares the elemental extraction of calcium *vs.* potassium (top), calcium *vs.* molybdenum (middle), and molybdenum *vs.* potassium (bottom) during the leaching experiments. In the calcium *vs.* potassium comparison for synthetic minerals, potassium leached far more than calcium (by percentage) for both akermanite and calcio-olivine, whereas the calcio-olivine samples showed more leaching of potassium *vs.* calcium than did akermanite, suggesting potential non-incorporation of potassium in the crystal structure of

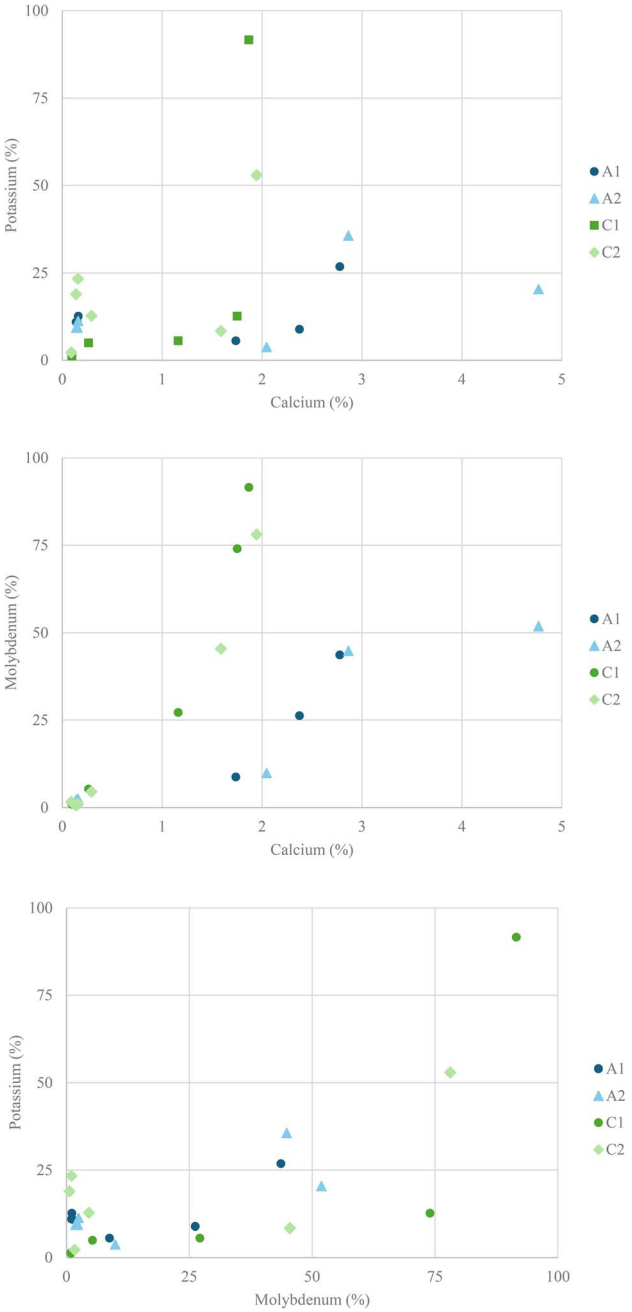

Fig. 13 The weathering results of akermanite and calcio-olivine samples indicating the extraction of calcium *vs.* potassium leaching (top), calcium *vs.* molybdenum leaching (middle), and molybdenum *vs.* potassium leaching (bottom).

akermanite. This finding also suggests that potassium is more readily available for leaching in the case of calcio-olivine than in the case of akermanite. In the calcium *vs.* molybdenum leaching comparison (Fig. 13), both the akermanite and calcio-olivine samples leached more molybdenum than calcium did (by percentage). It was found that akermanite leached more calcium than did calcio-olivine, which is consistent with the findings shown in Fig. 12. On the other hand, the calcio-olivine samples leached more molybdenum than did the akermanite

samples. When molybdenum leaching was compared with potassium leaching (Fig. 13), it was found that the calcio-olivine samples leached more molybdenum and potassium than did the akermanite samples. This analysis helps in understanding the incorporation fate of micronutrients (molybdenum and potassium) in the crystal structure of synthesized minerals, akermanite and calcio-olivine, as these micronutrients leach far more (by percentage) than calcium does.

Tables 5 and 6 present the values predicted by the trained machine learning model for the parameters required for computing the weathering rates of akermanite and calcio-olivine, respectively. Fig. 14 represents the forecasted weathering rates of akermanite and calcio-olivine along with enstatite, oligoclase, and K feldspar, described in $\log W_r$ (mol m^{-2} s^{-1}) as a function of the solution pH. Compared with akermanite, calcolivine has a greater (less negative) logarithmic weathering rate. In other words, calcio-olivine has a higher dissolution rate than akermanite does. Both the calcio-olivine and akermanite curves decrease with increasing pH, which suggests that acidic pH conditions weather more of these minerals than basic pH conditions do. The degree of decline of akermanite is also greater with increasing pH, indicating that the rate of weathering of akermanite decreases more than that of calcio-olivine when the pH of the solution moves from acidic to basic. Enstatite, oligoclase, and feldspar weather at a slower rate under acidic conditions, whereas the weathering of these minerals decreases to very low levels as the pH of the solution becomes basic.

Table 5 Machine learning-trained model-predicted parameters for akermanite

pH	$\log k$	E	$\log a$	n_{H^+}	$\log W_r$
3	−7.7583	146.7	17.9	0.2988	−8.7
3.5		146.7	17.9		−8.8
4		146.7	17.9		−9.0
4.5		146.7	17.9		−9.1
5		155.1	19.4		−9.3
5.5		155.1	19.4		−9.4
6		155.1	19.4		−9.6
6.5		155.1	19.4		−9.7
7		155.1	19.4		−9.8
7.5		197.3	26.8		−10.0
8		239.4	34.2		−10.1
8.5		239.4	34.2		−10.3
9		239.4	34.2		−10.4

Table 6 Machine learning-trained model-predicted parameters for calcio-olivine

pH	$\log k$	E	$\log a$	n_{H^+}	$\log W_r$
3	−7.7727	121.4	13.5	0.1568	−8.2
3.5		121.4	13.5		−8.3
4		121.4	13.5		−8.4
4.5		121.4	13.5		−8.5
5		121.4	13.5		−8.6
5.5		121.4	13.5		−8.6
6		121.4	13.5		−8.7
6.5		121.4	13.5		−8.8
7		121.4	13.5		−8.9
7.5		163.5	20.9		−8.9
8		205.7	28.3		−9.0
8.5		205.7	28.3		−9.1
9		205.7	28.3		−9.2

Fig. 15 represents cumulative CO_2 sequestration for 76 years per tonne per hector for synthetic (akermanite and calcio-olivine) and naturally occurring (oligoclase, K feldspar, enstatite) minerals. It is important to track the application of each tonne of mineral applied per hectare per year, which can be accomplished by computing the weathering/dissolution extent (X) and CO_2 drawdown capacity of each mineral. The mathematical modeling was conducted under ultraacidic (pH = 3.25), strongly acidic (pH = 5.25), and neutral (pH = 7.25) soil conditions. Both synthetic silicates, akermanite and calcio-olivine, capture more CO_2 than their naturally occurring silicate counterparts (oligoclase, K feldspar, and enstatite). Among synthetic silicates, calcio-olivine captures more CO_2 than akermanite does. One mole of calcio-olivine can potentially sequester two moles of CO_2 as carbonates, whereas one mole of akermanite can potentially sequester three moles of CO_2 as carbonates, two moles by releasing two calcium cations and one mole by releasing a single magnesium cation. However, the weathering rate of calcio-olivine is greater than that of akermanite, which places calcio-olivine in the leading position. This analysis indicated that the weathering rate is the governing parameter for identifying the CO_2 sequestration capabilities of minerals. Another key takeaway from this analysis is the prevalence of the weathering rate factor over the potential CO_2 sequestration capacity of a single mole of mineral, as akermanite, with three potential slots for CO_2 capture, lags from calcio-olivine, which has two potential slots for CO_2 capture. Fig. 16 shows the accumulation of CO_2 per year by synthesized and naturally occurring minerals, indicating relatively faster weathering and an improved capacity for CO_2 capture by synthesized minerals.

Fig. 17 shows a similar deployment analysis in which wollastonite, forsterite, and lizardite (naturally occurring silicate minerals) were applied at a rate of 1 tonne/hector/year from 2023 to 2100 (78 years), with soil pH values of ultra-acidic (3.25), strongly acidic (5.25) and neutral (7.25), respectively, while a uniform particle size of 100 μm was assumed (Haque *et al.*, 2023). While synthesized minerals (akermanite and calcio-olivine) performed better than oligoclase, K feldspar, and enstatite in terms of the cumulative CO_2 sequestered over a period of 76 years, they sounded comparably to assess carbon capture deployment with other naturally occurring minerals, such as wollastonite, feldspar, and lizardite (Haque *et al.*, 2023). Compared with Fig. 17, the performance of calcio-olivine was better than that of wollastonite under ultracidic conditions. Lizardite performed almost as well as calcio-olivine, whereas forsterite, it performed better than calcio-olivine. When examining the reaction kinetics data of Palandari *et al.* (2004), many extrapolations have been made to prepare the data, and extensive and comprehensive experiments are needed to determine the number of samples present in their study. Another reason

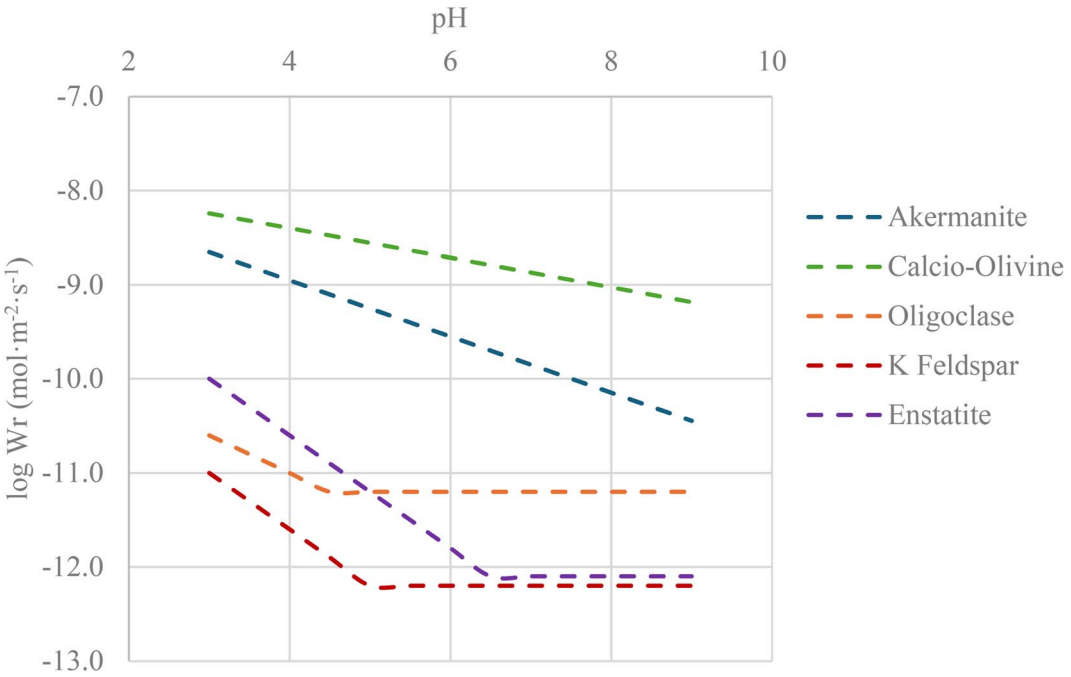

Fig. 14 The forecasted weathering rates of synthesized minerals predicted by the trained machine learning model plotted along with naturally occurring minerals such as oligoclase, K feldspar, and enstatite.

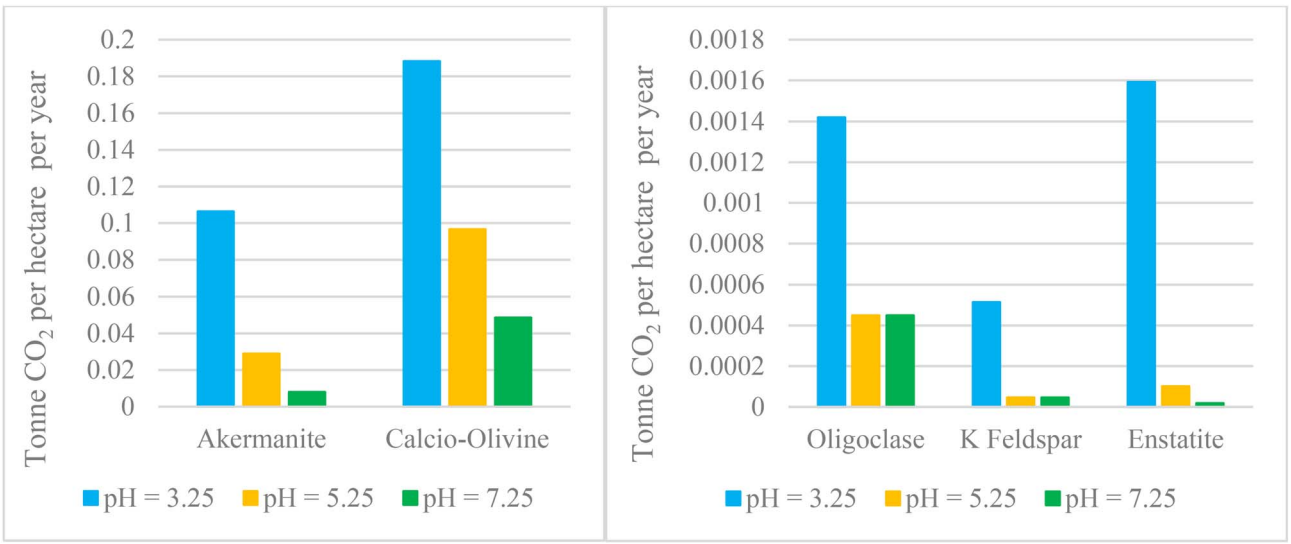

Fig. 15 Tonne CO_2 per hectare per year for (left) akermanite and calcio-olivine and (right) oligoclase, K feldspar, and enstatite.

that forsterite performs better than calcio-olivine could be that the machine learning model was not thorough enough to predict the weathering rates of minerals precisely in this study. Training the machine learning model with an increased number of datasets can help in curing the model enough to predict more reliable numbers. The difference between calcio-olivine and forsterite is the presence of two atoms of calcium present in one molecule of calcio-olivine and two atoms of magnesium in a molecule of forsterite. The ionic potential of calcium is 2.02, and that of magnesium is 3.077, which could make it more feasible for magnesium to interact with water molecules and become part of the solution. Other factors that could influence the leaching of magnesium over that of calcium include the increased hydration energy and mobility of magnesium cations in water compared with those in calcium. Keeping these insights in view of rigorous experiments and comprehensive datasets can provide certainty to the weathering behavior of these naturally occurring and silicate minerals.

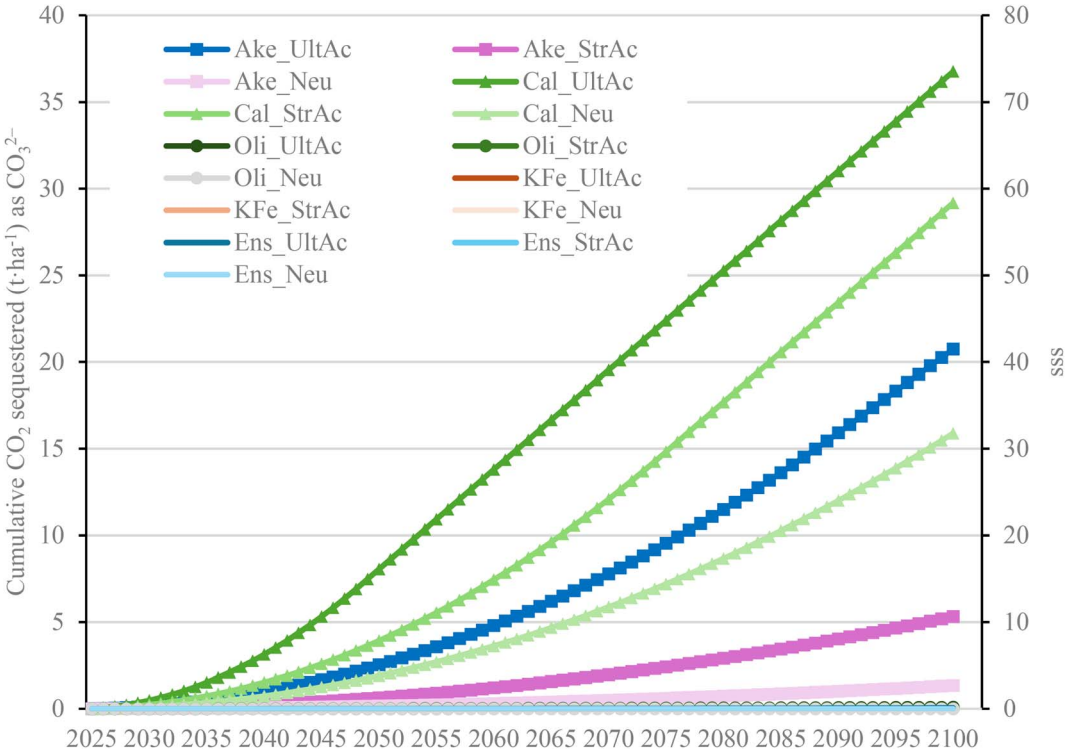

Fig. 16 Cumulative CO_2 sequestration trends of synthetic (akermanite (Ake) and calcio-olivine (Cal)) and naturally occurring (oligoclase (Oli), K Feldspar (KFe), and enstatite (Ens)) silicates applied at rates of 1 tonne/hector/year from 2025–2100 (for 76 years) with soil pH values of ultra-acidic (3.25), strongly acidic (5.25) and neutral (7.25) while assuming a uniform particle size of 100 μm.

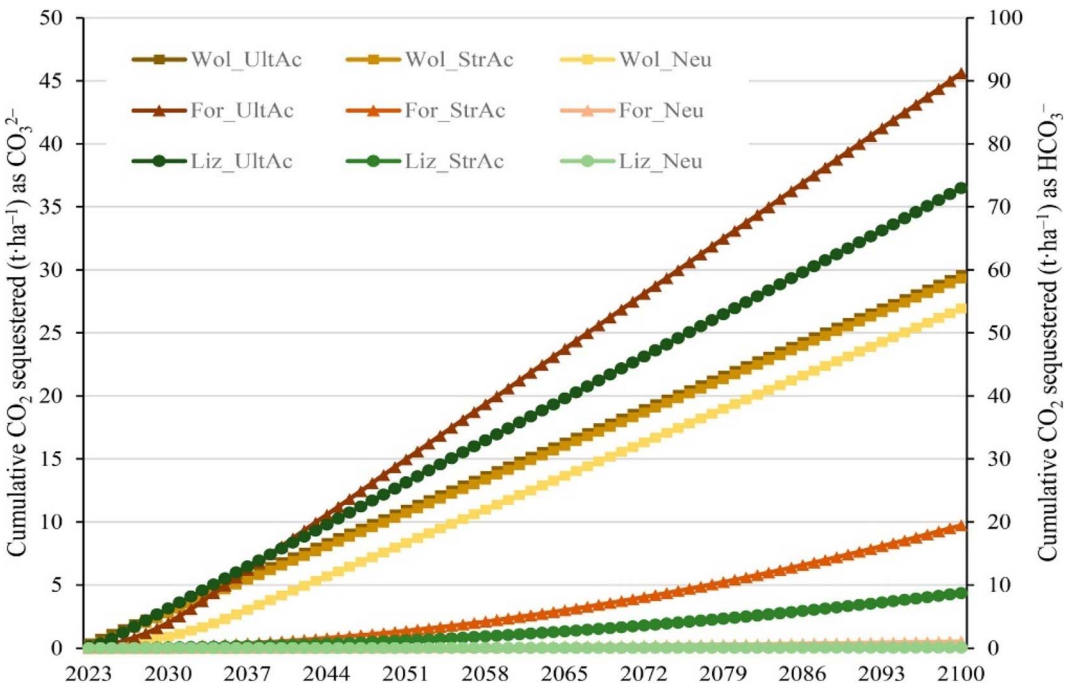

Fig. 17 Cumulative CO_2 sequestration trends of naturally occurring silicate minerals (wollastonite, forsterite, lizardite) applied at a rate of 1 tonne/hector/year from 2023 to 2100 (for 78 years) with soil pH values of ultra-acidic (3.25), strongly acidic (5.25) and neutral (7.25) while assuming a uniform particle size of 100 μm (Haque *et al.*, 2023). CC-BY.

Conclusions

The present work investigated the synthesis and weathering process of nutrient-doped silicate minerals during fast weathering through solid-state sintering methodology. A solid-state sintering methodology was used to synthesize akermanite and calcio-olivine doped with plant nutrients. The synthesis process followed by XRD, SEM, and SEM-EDS characterization analysis confirmed the success of the methodology. Weathering experiments were conducted in conjunction with wollastonite, olivine, feldspar, and serpentine to obtain a comparison overview of how fast synthetic minerals are leaching compared with naturally occurring silicate minerals. The results include:

-Faster leaching of calcium ions from synthesized minerals than from naturally occurring silicate minerals. During the later stages of weathering, the amount of calcium ions leached from synthetic minerals is lower than that leached from naturally occurring silicate minerals, indicating the rapid weathering of silicate minerals.

-Leaching of calcium ions from synthesized minerals was faster in the early stages of weathering, followed by slow leaching in the later stages of the experiments.

-Leaching results revealed greater release of potassium and molybdenum than of calcium (by percentage) for both minerals. This finding indicates that both potassium and molybdenum were possibly unable to be present in the crystal structure of akermanite and calcio-olivine.

-Calcio-olivine released more potassium and molybdenum (by percentage) than did akermanite.

-Future research directions include investigating more synthesis methodologies for micro-nutrients' incorporation such that their release becomes relatively slow and can promote plant development.

-Machine learning model's predicted weathering rates indicated better weathering for calcio-olivine than for akermanite, where the rate of degradation of weathering with increasing pH was lower for calcio-olivine than for akermanite.

-Shrinking core mathematical model with the application rate of 1 tonne/hector/year of each mineral for 76 years from 2025 to 2100 resulted in more CO_2 capture by synthetic silicate minerals than by naturally occurring silicate minerals.

These results will help the scientific community understand the weathering behavior of minerals and open further avenues for research in the domain of enhanced rock weathering of silicate minerals.

Conflicts of interest

There are no conflicts to declare.

Data availability

The datasets generated and analyzed during this study are available from the corresponding author upon reasonable request.

Supplementary information (SI): mathematica code used for developing the machine learning model. See DOI: https://doi.org/10.1039/d5va00394f.

Acknowledgements

This research was funded by Scialog®, Research Corporation for Science Advancement (RCSA), Natural Science and Engineering Research Council (Discovery Grant) and Thistledown Foundation: 2768.

References

1 Climate Change 2022: Impacts, Adaptability and Vulnerability, 2022.
2 S. Zhang, S. Jiang, H. Li, P. Li, X. Zhong, C. Chen, G. Tu, X. Liu and Z. Xu, Current Status and Reflections on Ocean CO2 Sequestration: A Review, *Energies*, 2025, **18**(4), 942, DOI: 10.3390/en18040942.
3 H. S. Jung, B. G. Kim, J. H. Kwon and J. W. Bae, Thermocatalytic technologies for syngas production from greenhouse gases and biomass-derived renewable oxygenates, *Renew. Sustain. Energy Rev.*, 2025, **216**, 115711, DOI: 10.1016/j.rser.2025.115711.
4 H. S. Jung, B. G. Kim and J. W. Bae, Synthetic routes of clean hydrocarbons fuels and oxygenates by catalytic conversions of carbon oxides, *Appl. Catal. B Environ.*, 2024, **343**, 123477, DOI: 10.1016/j.apcatb.2023.123477.
5 H. K. Jeswani, D. M. Saharudin and A. Azapagic, Environmental sustainability of negative emissions technologies: A review, *Sustain. Prod. Consum.*, 2022, **33**, 608–635, DOI: 10.1016/j.spc.2022.06.028.
6 F. J. R. Meysman and F. Montserrat, Negative CO_2 emissions via enhanced silicate weathering in coastal environments, *Biol. Lett.*, 2017, **13**(4), 28381634, DOI: 10.1098/rsbl.2016.0905.
7 C. Dietzen and M. T. Rosing, Quantification of CO_2 uptake by enhanced weathering of silicate minerals applied to acidic soils, *Int. J. Greenh. Gas Control*, 2023, **125**, 103872, DOI: 10.1016/j.ijggc.2023.103872.
8 R. Tan, K. B. Aviso, S. Bandyopadhyay, *et al.*, Circular economy meets the drawdown economy: Enhanced weathering of industrial solid waste as a win-win solution, *Resour. Conserv. Recycl.*, 2022, **178**, 106029, DOI: 10.1016/j.resconrec.2021.106029.
9 A. Ali, Y. W. Chiang and R. M. Santos, Synthesis of fast-weathering nutrient-doped silicate minerals and their prospect as a negative emissions technology, *COM 2022: Proceedings of the 61st Conference of Metallurgists*, 2022, 53–57, DOI: 10.1007/978-3-031-17425-4_10.
10 P. Smith, S. J. Davis, F. Creutzig, *et al.*, Biophysical and economic limits to negative CO_2 emissions, *Nat. Clim. Change*, 2016, **6**, 42–50, DOI: 10.1038/nclimate2870.
11 P. Renforth, J. Edmondson, J. R. Leake, *et al.*, Designing a carbon capture function into urban soils, *Proc. ICE - Urban Des. Plan.*, 2011, **164**(2), 121–128, DOI: 10.1680/udap.2011.164.2.121.

12 C.-L. Washbourne, E. L-Capel, P. Renforth, *et al.*, Rapid removal of atmospheric CO_2 by urban soils, *Environ. Sci. Technol.*, 2015, **49**(9), 5434–5440, DOI: 10.1021/es505476d.
13 D. A. C. Manning, P. Renforth, E. L-Capel, *et al.*, Carbonate precipitation in artificial soils produced from basaltic quarry fines and composts: An opportunity for passive carbon sequestration, *Int. J. Greenh. Gas Control*, 2013, **17**, 309–317, DOI: 10.1016/j.ijggc.2013.05.012.
14 S. Kumar, A. Kumar and A. Mandal, Characterizations of surfactant synthesized from Jatropha oil and its application in enhanced oil recovery, *AIChE J.*, 2017, **63**(7), 27312741, DOI: 10.1002/aic.15651.
15 M. Bai, Z. Zhang and X. Fu, A review on well integrity issues for CO_2 geological storage and enhanced gas recovery, *Renew. Sustain. Energy Rev.*, 2016, **59**, 920–926, DOI: 10.1016/j.rser.2016.01.043.
16 S. Park, CO_2 reduction-conversion to precipitates and morphological control through the application of the mineral carbonation mechanism, *Energy*, 2018, **153**, 413–421, DOI: 10.1016/j.energy.2018.04.086.
17 J. S. Lee and E. C. Choi, CO_2 leakage environmental damage cost - A CCS project in South Korea, *Renew. Sustain. Energy Rev.*, 2018, **93**, 753–758, DOI: 10.1016/j.rser.2018.04.074.
18 W. Seifritz, CO_2 disposal by means of silicates, *Nature*, 1990, **345**, 486, DOI: 10.1038/345486b0.
19 Q. Liu, L. Teng, S. Rohani, *et al.*, CO_2 mineral carbonation using industrial solid wastes: A review of recent developments, *Chem. Eng. J.*, 2021, **416**, 129093, DOI: 10.1016/j.cej.2021.129093.
20 S. Pandey, V. C. Srivastava and V. Kumar, Comparative thermodynamic analysis of CO_2 based dimethyl carbonate synthesis routes, *Can. J. Chem. Eng.*, 2021, **99**(2), 467–478, DOI: 10.1002/cjce:23893.
21 S. Sanna, W. Schmidt and P. Thissen, Formation of Hydroxyl Groups at Calcium-Silicate-Hydrate (C-S-H): Coexistence of Ca-OH and Si-OH on Wollastonite (001), *J. Phys. Chem. C*, 2014, **118**, 8007–8013, DOI: 10.1021/jp500170t.
22 F. Haque, R. M. Santos, A. Dutta, *et al.*, Co-benefits of wollastonite weathering in agriculture: CO_2 sequestration and promoted plant growth, *ACS Omega*, 2019, **4**, 1425–1433, DOI: 10.1021/acsomega.8b02477.
23 M. Z. Kashim, H. Tsegab, O. Rahmani, *et al.*, Reaction Mechanism of Wollastonite in situ Mineral Carbonation for CO_2 Sequestration: Effects of Saline Conditions, Temperature, and Pressure, *ACS Omega*, 2020, **5**(45), 28942–28954, DOI: 10.1021/acsomega.0c02358.
24 X. Xu, W. Liu, G. Chu, *et al.*, Energy-efficient mineral carbonation of CaSO4 derived from wollastonite via a roasting-leaching route, *Hydrometallurgy*, 2019, **184**, 151–161, DOI: 10.1016/j.hydromet.2019.01.004.
25 F. Di-Lorenzo, C. Ruiz-Agudo, A. Ibanez-Velasco, *et al.*, The carbonation of wollastonite: A model reaction to test natural and biomimetic catalysts for enhanced CO_2 sequestration, *Minerals*, 2018, **8**, 209, DOI: 10.3390/min8050209.
26 S. Yadav and A. Mehra, Mathematical modelling and experimental study of carbonation of wollastonite in the aqueous media, *J. CO_2 Util.*, 2019, **31**, 181–191, DOI: 10.1016/j.jcou.2019.03.013.
27 J. H. Kwak, J. Z. Hu, R. V. F. Turcu, *et al.*, The role of H_2O in the carbonation of forsterite in supercritical CO_2, *Int. J. Greenh. Gas Control*, 2011, **5**(4), 1081–1092, DOI: 10.1016/j.ijggc.2011.05.013.
28 H. T. Schaef, B. P. McGrail, J. L. Loring, *et al.*, Forsterite [Mg2SiO4)] carbonation in wet supercritical CO_2: An in situ high-pressure X-ray diffraction study, *Environ. Sci.*, 2013, **47**(1), 174–181, DOI: 10.1021/es301126f.
29 J. Laonamsai, P. Tasi, P. Wiwatrojanagul, *et al.*, Synergistic effects of CuO and CaF_2 additives in facilitating low-temperature tricalcium silicate formation and stabilization, *Results Eng.*, 2025, **26**, 104620, DOI: 10.1016/j.rineng.2025.104620.
30 W. Liu, G. Chu, H. Yue, *et al.*, Phase Equilibrium of the MgSO4-(NH4)2SO4-H2O ternary system: Effects of sulfuric acid and iron sulfate and its application in mineral carbonation of serpentine, *J. Chem. Eng. Data*, 2018, **63**, 1603–1612, DOI: 10.1021/acs.jced.7b01113.
31 S. Lavikko and O. Eklund, The significance of the serpentinite characteristics in mineral carbonation by "the ÅA Route", *Int. J. Miner. Process.*, 2016, **152**, 7–15, DOI: 10.1016/j.minpro.2016.04.009.
32 I. S. Ramao, L. M. Gando-Ferreira, M. M. V. G. da Silva, *et al.*, CO_2 sequestration with serpentinite and metaperidotite from Northeast Portugal, *Miner. Eng.*, 2016, **94**, 104–114, DOI: 10.1016/j.mineng.2016.05.009.
33 X. Wang and M. M. Maroto-Valer, Integration of CO_2 capture and mineral carbonation by using recyclable ammonium salts, *ACS Sustainable Chem. Eng.*, 2011, **4**(9), 1291–1300, DOI: 10.1002/cssc.201000441.
34 X. Wang and M. M. Maroto-Valer, Dissolution of serpentine using recyclable ammonium salts for CO_2 mineral carbonation, *Fuel*, 2011, **90**(3), 1229–1237, DOI: 10.1016/j.fuel.2010.10.040.
35 C.-U. Kang, S.-W. Ji and H. Jo, Recycling of industrial waste gypsum using mineral carbonation, *Sustainability*, 2022, **14**(8), 4436, DOI: 10.3390/su14084436.
36 H.-P. Mattila and R. Zevenhoven, Mineral carbonation of phosphogypsum waste for production of useful carbonate and sulfate salts, *Front. Energy Res.*, 2015, **3**, 48, DOI: 10.3389/fenrg.2015.00048.
37 W. Tan, Z. Zhang, H. Li, *et al.*, Carbonation of gypsum from wet flue gas desulfurization process: Experiments and modeling, *Environ. Sci. Pollut. Res.*, 2017, **24**, 8602–8608, DOI: 10.1007/s11356-017-8480-0.
38 I. Ngo, L. Ma, *et al.*, Enhancing fly ash utilization in backfill materials treated with CO_2 carbonation under ambient conditions, *Int. J. Min. Sci. Technol.*, 2023, **33**(3), 323–337, DOI: 10.1016/j.ijmst.2023.02.001.
39 Q. Yuan, Y. Zhang, T. Wang, *et al.*, Characterization of heavy metals in fly ash stabilized by carbonation with supercritical CO_2 coupling mechanical force, *J. CO2 Util.*, 2023, **67**, 102308, DOI: 10.1016/j.jcou.2022.102308.
40 H.-J. Ho, A. Iizuka and E. Shibata, Utilization of low-calcium fly ash via direct aqueous carbonation with a low-energy

input: Determination of carbonation reaction and evaluation of the potential of CO_2 sequestration and utilization, *J. Environ. Manage.*, 2021, **288**, 112411, DOI: 10.1016/j.jenvman.2021.112411.

41 C. Yu, C. Cui, J. Zhao, *et al.*, Carbonation properties of dredged slurry pre-dried with steel slag powder: Effects of clay minerals and organic acids, *Constr. Build. Mater.*, 2022, **353**, 129096, DOI: 10.1016/j.conbuildmat.2022.129096.

42 R. M. Santos, J. V. Bouwel, E. Vandevelde, *et al.*, Accelerated mineral carbonation of stainless steel slags for CO_2 storage and waste valorization: Effects of process parameters on geochemical properties, *Int. J. Greenh. Gas Control*, 2013, **17**, 32–45, DOI: 10.1016/j.ijggc.2013.04.004.

43 W. J. J. Huijgen, G.-J. Witkamp and R. N. J. Comans, Mineral CO_2 sequestration by steel slag carbonation, *Environ. Sci. Technol.*, 2005, **39**(24), 9676–9682, DOI: 10.1021/es050795f.

44 Q. Liu, W. Liu, J. Hu, *et al.*, Energy-efficient mineral carbonation of blast furnace slag with high value-added products, *J. Clean. Prod.*, 2018, **197**(1), 242–252, DOI: 10.1016/j.jclepro.2018.06.150.

45 J. Gao, C. Li, W. Liu, *et al.*, Process simulation and energy integration in the mineral carbonation of blast furnace slag, *Chin. J. Chem. Eng.*, 2019, **27**(1), 157–167, DOI: 10.1016/j.cjche.2018.04.012.

46 Z. Liu, P. V. D. Heede, C. Zhang, *et al.*, Carbonation of blast furnace slag concrete at different CO_2 concentrations: Carbonation rate, phase assemblage, microstructure and thermodynamic modelling, *Cem. Concr. Res.*, 2023, **169**, 107161, DOI: 10.1016/j.cemconres.2023.107161.

47 A. S. S. Nedunuri, A. Y. Mohammed and S. Muhammad, Carbonation potential of concrete debris fines and its valorisation through mineral carbonation, *Constr. Build. Mater.*, 2021, **310**, 125162, DOI: 10.1016/j.conbuildmat.2021.125162.

48 M. Zajac, J. Skibsted, F. Bullerjahn, *et al.*, Semi-dry carbonation of recycled concrete, *J. CO2 Util.*, 2022, **63**, 102111, DOI: 10.1016/j.jcou.2022.102111.

49 US Geological Survey USGS, *Miner. Commod. Summ.*, 2020, DOI: 10.3133/mcs2020.

50 S.-Y. Pan, Y.-H. Chen, L.-S. Fan, *et al.*, CO_2 mineralization and utilization by alkaline solid wastes for potential carbon reduction, *Nat Sustainability*, 2020, **3**, 399–405, DOI: 10.1038/s41893-020-0486-9.

51 M. L. Jackson and G. Donal Sherman, Chemical weathering of minerals in soils, *Adv. Agron.*, 1953, **5**, 219–318, DOI: 10.1016/S0065-2113(08)60231-X.

52 M. Bodor, R. M. Santos, L. Kriskova, J. Elsen, M. Vlad and T. V. Gerven, Susceptibility of mineral phases of steel slags towards carbonation: mineralogical, morphological and chemical assessment, *Eur. J. Mineral.*, 2013, **25**(4), 533–549.

53 A. Ali, Y. W. Chiang and R. M. Santos, X-ray diffraction techniques for mineral characterization: A review for engineers of the fundamentals, applications, and research directions, *Minerals*, 2022, **12**(2), 205, DOI: 10.3390/min12020205.

54 A. Ali, N. Zhang and R. M. Santos, Mineral Characterization Using Scanning Electron Microscopy (SEM): A Review of the Fundamentals, Advancements, and Research Directions, *Appl. Sci.*, 2023, **13**(23), 12600, DOI: 10.3390/app132312600.

